Carbon 163 (2020) 197–201

Contents lists available at ScienceDirect

Carbon

journal homepage: www.elsevier.com/locate/carbon

Letter to the editor

All-carbon THz components based on laser-treated diamond

A B S T R A C T

We report on fs laser structuring and graphitization of diamond and experimental characterization of its THz response. A full characterization of graphitized, conductive layer generated by laser irradiation is carried out by performing scanning-electron microscopy, Raman spectroscopy and electrical measurements. The transmittance of the laser textured diamond samples, both with the graphitic overlayer and after selective oxidizing etching, is analyzed in the (0.25 ÷ 6.0) THz spectral range. A significant selective absorption of the graphitized overlayer towards polarized THz radiation is demonstrated, which is associated to the formation of graphitic laser induced periodic surface structures. This anisotropy allows conceiving compact passive metasurfaces based on conductive/dielectric patterns on the diamond plate surface for the development of robust, lightweight and broadband THz optical components.

Diamond and graphite are two of the allotropes of carbon with extremely different physical properties arising from their distinct crystal structures. For example, diamond is optically transparent and an electrical insulator, whereas graphitic phases of carbon are optically opaque and may transport efficiently electrical current. Recently, laser processing and induced graphitization of diamond is opening up interesting routes in manufacturing new elements in photonics, electronics, energy conversion, etc. [1–5]. In fact, the very different electrical and optical properties between diamond and graphitic-like materials coupled to the versatility of the laser processing approaches can make possible adding new functionalities by engineering a diamond crystal at the surface or in the volume [4,6–9]. This might be exploited to develop sub-wavelength structures for the manipulation of surface plasmon polaritons or photonic crystals with a corrugated surface showing superlensing properties [10,11], to name a few examples.

Femtosecond (fs) laser irradiation has already shown interesting results in the improvement of the THz emission and transmission response of a material, as for example in the case of GaAs [12,13]. In particular, Zhao et al. reported on an anisotropic response to THz radiation induced by the formation of laser induced periodic surface structures (LIPSS) on GaAs [13]. The generation of LIPSS is a characteristic phenomenon associated to fs laser irradiation of solid target materials [14,15], and it has been reported also for diamond [5,16–19]. The LIPSS formation is typically explained in terms of the interference of the incident laser and surface scattered waves related to the excited electrons and plasmonic excitation induced during multi-pulse fs laser irradiation. Various kind of LIPSS can be formed [14] and those induced in the case of diamond irradiated by ultrashort laser pulses in various experimental conditions were recently reviewed in Ref. [5]. The more common LIPPS, generally indicated as ripples, show a typical period equal to $\lambda_L/2n$, being λ_L the laser wavelength and n the refractive index of the target material.

While the optical properties of diamond are well established in a wide spectral range [1,20], the characterization of the electromagnetic (EM) response of the graphitized layers produced by fs laser irradiation of diamond is still scarcely investigated [4,21].

Here we report an experimental investigation on the transmittance in the THz spectral range of diamond films laser-irradiated by ultrashort laser pulses. Our study is motivated by the increasing interest in THz technologies and the demand of new optoelectronic components and devices enhancing the capability either of manipulating light and EM waves or of collecting their energy. Diamond is an ideal material for THz technology because it is very transparent in the visible range as well as in the full THz range (0–30 THz), while graphite is (like any conductor) strongly absorbing. The combination of these two materials, with a tailored long-range order, is therefore likely to allow the design of new THz-optics devices. Since micromachining of the robust diamond lattice with standard microelectronics technique is a rather hard task, laser-induced modifications may provide an alternative approach. In particular, the effective possibility to create graphitized islands in the diamond lattice represents a key-tool in the development of THz metamaterial components.

Fs laser irradiation of diamond has already allowed the tailoring of diamond optical properties [3,22] and the development of black diamond films for solar energy conversion [16,23] with enhanced optical absorptance in the UV-VIS-NIR range and drastically improved sub-bandgap responsivity. Exploiting surface graphitization, the response of fs laser processed diamond can be investigated also in the THz region, thus assessing the viability of diamond as a route towards an all-carbon platform for THz metamaterials.

Here diamond samples are irradiated with fs laser pulses

https://doi.org/10.1016/j.carbon.2020.03.023
0008-6223/

producing a graphitized, conductive overlayer on the complete surface. Black diamond samples are also obtained by selective oxidizing wet etching after laser irradiation. Both classes of structured materials are characterized by field-emission scanning-electron microscopy (FE-SEM), Raman spectroscopy and electrical measurements. Their EM response is analyzed in the (0.25 ÷ 6.0) THz range by exploiting THz Time-Domain-Spectroscopy (TDS). Two different TDS systems for generating and detecting THz pulses were used both to improve the soundness of the experimental findings and characterize the samples over a wide spectral range. The observed results, given in terms of transmittance, demonstrate a significant selective absorption of the graphitic overlayer towards polarized THz radiation.

We used as starting material free-standing 10×10 mm^2 thermal grade, polycrystalline, CVD diamond plates, produced by Element Six Ltd, with a thickness of 250 μm, a surface roughness lower than 50 nm, and a bulk resistivity of the order of 10^{15} Ωcm. The laser source is a Ti:Sapphire system delivering 800 nm linearly polarized laser pulses with a duration of ≈100 fs at a repetition rate of 1 kHz. The diamond target is held on a XY translation stage located in a high vacuum chamber ($<10^{-7}$ mbar) perpendicularly to the laser optical path and laser processed over an area of about 9.5×9.5 mm^2 through appropriate sample scanning. The variation of experimental parameters (e.g. translation speed, pulse fluence, etc.) allows inducing different modifications to the diamond sample surface. In the present study, we measure the THz response of laser irradiated diamond by selecting two twin samples processed by using the same experimental conditions. In particular, laser pulses with energy of 3.6 mJ are focused on the sample surface to a spot diameter of the Gaussian laser beam (at $1/e^2$ of its maximum intensity) of ≈250 μm. The sample target is moved at a scanning speed of 0.75 mm/s to form longitudinal lines, with a longitudinal overlap of about 99.5% and a number of overlapped pulses of ≈330. A line-to-line separation $P = 75$ μm is used in the laser treatments. These parameters induce a total accumulated fluence released on the sample of 5.0 kJ/cm^2, i.e. the experimental conditions for the production of high performance black diamond [23]. After the laser treatments, a first sample is processed by a selective oxidizing etching (solution of H_2SO_4:$HClO_4$:HNO_3 in the 1:1:1 ratio, 15 min at boiling point) in order to remove the graphitic overlayer [16], thus obtaining a reference black diamond (BD) sample. The second one is left as treated and indicated as graphitized diamond (GD) hereafter.

Fig. 1 reports FE-SEM cross-sectional images of the cross-sections of the two samples obtained with a Leo Supra-35 model. Panel (a) of Fig. 1 illustrates the morphological features of the graphitized sample evidencing the formation of a compact graphitic overlayer with a thickness of about 700–800 nm over the diamond plate. The zoomed view (panel (b)) better shows the texture of the surface in form of a corrugated overlayer covering diamond LIPSS. Panel (c) reports a cross section of the BD sample obtained after selective removal of sp^2 carbon and displaying the characteristic surface diamond LIPSS with a height of about 250 nm. Interestingly, both the graphitic cover and the underlying diamond ripples show the same spatial disposition, perpendicularly to the laser beam polarization, and a period $L \approx 170$ nm [16,23]. The nanoparticles observed in panel (c) are due to the conductive layer of gold coating covering the black diamond sample for the FE-SEM measurements.

Fig. 2 reports the Raman spectra taken on the GD (panel a) and BD (panel b) samples, at room temperature with an Ar^+ laser (514.5 nm) in back-scattering geometry. The measurements were carried out by using a Dilor XY triple spectrometer (1 cm^{-1} resolution) equipped with a liquid nitrogen cooled charge coupled device detector. A customized system with an adapted Olympus microscope arranged in confocal mode allows to obtain a spot size of 2 μm. The Raman spectrum the GD sample displays characteristic signatures of carbon phases with two broad peaks at 1380 cm^{-1} (D band, associated to the breathing mode of sp^2 hybridization in aromatic chains, taking into account the disorder in sp^3/sp^2 carbon bonds) and 1580 cm^{-1} (G band, associated to the stretching vibration of the sp^2 hybridization in carbon-carbon bonds and aromatic chains) [24], without any signal from the underlying diamond due to the strong absorption of the exciting photons by the thick graphitic overlayer covering the GD sample. The ratio between the intensities of the two bands I_D/I_G is about 1.33, thus indicating an almost similar contribution of sp^2 and sp^3 carbon allotropes [25]. Similar features have been observed earlier in the Raman spectrum both of CVD diamond plates irradiated by KrF excimer laser pulses and hydrogenated amorphous carbon thin films irradiated by fs laser pulses [21,26].

Fig. 2(b) reports the Raman signal registered on the BD sample, with an intense characteristic diamond peak at 1332 cm^{-1} [27], over a noisy background indicating no evidence of sp^2 contribution and confirming that all surface graphitic-based contents are removed by the wet etching.

The electrical resistivity of the samples is characterized using a Van der Pauw method [28]. The graphitized layer on the GD sample is stable and homogenous on the surface, and electrically active with an overall extremely conductive behavior in many repeatable

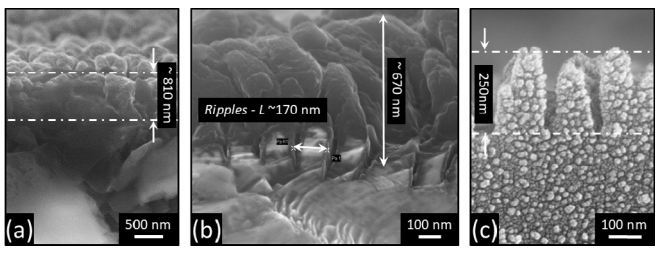

Fig. 1. SEM images of panels (a) and (b) show the cross-section of graphitized diamond at two different magnifications; panel (c) displays the diamond LIPSS left on the BD sample surface after selective oxidizing etching. (A colour version of this figure can be viewed online.)

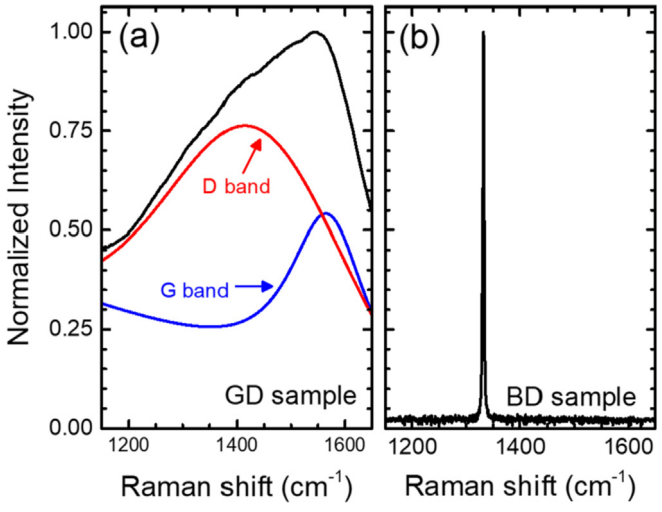

Fig. 2. Raman spectra recorded at room temperature for the GD (panel a) and BD (panel b) samples. The intensity was normalized to each maximum value. In panel (a) the black curve shows the measured Raman profile that is deconvoluted in the two characteristic D and G bands of graphitic phases. (A colour version of this figure can be viewed online.)

cycles of measurements. Its resistivity is $\approx 8 \times 10^{-3}\ \Omega$ cm, that well compares with typical values ($\approx 10^{-4}\ \Omega$ cm) for highly oriented pyrolytic graphite. On the contrary, the electrical resistivity of the BD sample is larger than $10^5\ \Omega$ cm (ten orders of magnitude lower than bulk resistivity of the pristine diamond samples), likely due to the presence of defects within the diamond bandgap [29].

The THz response of the samples is characterized by means of two different TDS systems. The first one (TDS-1) exploits a standard setup based on photo-conducting antennas excited by a ≈90 fs laser pulses at 1560 nm and generating a transient electric field pulses of 1–2 ps (Tera-K15, Menlo Systems) that provides measurements in the range 0.2–1.5 THz with a resolution of about 2.5 GHz. The second system (TDS-2), instead, produces broadband THz pulses through air-plasma generation by using a high-power regenerative Ti:Sappire amplifier (≈4 W, 800 nm, 35 fs, 1 kHz repetition rate) [30]. The generated radiation is filtered by means of a high resistivity thick silicon wafer, removing any unwanted radiation, and detected by means of electrooptic sampling in an LAPC (Lemke/amorphous polycarbonate) electrooptic polymer. This allows investigating the THz response of the sample in the spectral range 0.5–6 THz. From the comparison with the reference electric fields, the transmittance T of the samples is obtained with both setups. The measurements are carried out in a dry nitrogen environment in order to reduce any possible influence from water vapor contributions in the recorded signals.

As a reference, the transmission of an untreated diamond plate is also measured (not shown), observing an average transmissivity of ≈70% and an oscillating behavior of T as a function of frequency ν, due to the Fabry-Perot (etalon) effect, with maxima separated by a spectral distance $\Delta\nu \approx 0.25$ THz, consistently with a refractive index of diamond of 2.376 [4].

The transmittance T of the laser processed diamond samples is measured for impinging THz beam polarization parallel and perpendicular to the ripples formed on the laser structured samples (see Fig. 3(a)). The variation of T vs ν recorded by the TDS-1 and TDS-2 setups is reported in Fig. 3, panels (b) and (c) for GD and (d) and (e) for BD samples, respectively.

We illustrate first the THz response of the GD sample. In Fig. 3(b) and (c) one can observe a drastic reduction of the transmittance for the GD sample for both polarizations and a damping of the oscillation amplitude, because of the absorption produced by the graphitic overlayer. Strikingly, a clear anisotropy in the THz transmittance occurs for polarizations parallel ($T_{||}$) and perpendicular ($T_{\perp}$) to ripples orientation. In particular, $T_{||}$ reduces to a value of the order of ≈10% over the investigated range. This is consistent with the value of the transmittance of a homogeneous graphitized film (thickness ≈580 nm) produced on a diamond plate by KrF excimer laser (≈20 ns) irradiation recently reported by Komlenok et al. around 1 THz [4]. Instead, $T_{\perp}$ is much larger all over the investigated spectral range, thus evidencing a clear influence of the graphitic overlayer morphology on the THz response of the sample. These experimental observations suggest that the formation of a rippled, graphitic layer by fs laser irradiation on the diamond surface imparts a linear dichroism to the sample leading to a strong anisotropic response to THz radiation. In particular, the measured transmittance values indicate that the degree of polarization, DOP=$(T_{\perp}-T_{||})/(T_{\perp}+T_{||})$, of the GD sample has an average value of (65 ± 5)% for TDS-1 and (62 ± 6)% for TDS-2 spectral ranges. While such a figure is still too low to compete with conventional metal grid polarizers, due to the higher electrical conductivity of metals, it is nevertheless a promising outcome with significant room for improvements by appropriate design and optimization of the fs laser graphitized diamond structure.

We turn now to the THz response of the BD sample, whose transmittance is reported in Fig. 3(d) and (e). T anisotropy is also observed in the BD sample, due to the presence of the ripples

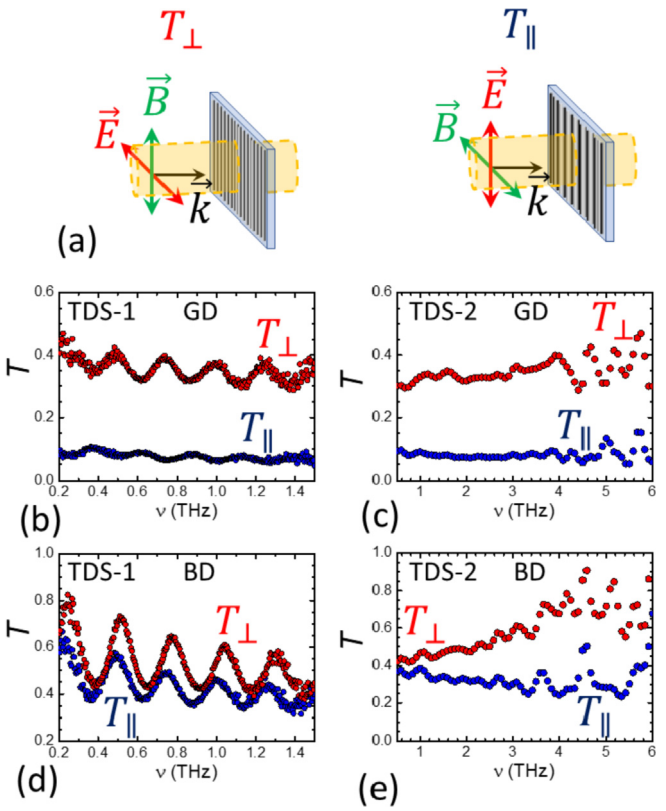

Fig. 3. Panel (a): sketch of the THz wave for THz electric field polarization orthogonal ($T_{\perp}$, red symbols) parallel ($T_{||}$, blue symbols) to the LIPSS. Panel (b–e): transmittance of graphitized (b–c) and black (d–e) diamond as taken using TDS-1 (left) and TDS-2 (right) setups. (A colour version of this figure can be viewed online.)

decorating the sample surface after the removal of the graphitized layer. Nevertheless, this anisotropy is largely reduced in the narrower spectral range of the TDS-1, whereas it is still pronounced at the higher frequencies probed by the TDS-2 systems.

It is worth to observe that increasing the frequency the transmittance of both GD and BD samples starts acquiring a noisy profile without modifying in any way the overall behavior. We ascribe this behavior to the presence of the "mesoscopic" periodicity P related to the laser writing process present on the samples surface that might be responsible for the onset of diffraction anomalies at frequencies above $f_P = \frac{c}{P} \approx 4$ THz [31,32]; however more investigations are desirable to thoroughly address this specific issue.

The experimental observation in the lower frequency range of TDS-1 clearly suggests that most of the difference in transmission observed for the GD sample at the two THz field polarizations is due to the sub-wavelength ordering of the graphitic overlayer. In an attempt to better gather the THz properties of the graphitic overlayer produced by fs laser surface texturing, we consider a very simplified, heuristic model of the complex GD sample. This sample can be depicted as a double layer consisting of a film of graphitic carbon on the top of a black diamond substrate. In this scenario, the transmission through the GD double layer can be derived by considering the transmissivities of the graphitic layer (GL), T_{GL}, and of the BD sample, T_{BD}. Since the total transmissivities of both GD and BD samples are measured, one can eventually work out the transmittance of the graphitized layer T_{GL} as:

$$T_{GL} = \frac{T_{GD}}{T_{BD}} = e^{-\alpha_{GL} d_{GL}} \quad (1)$$

where α_{GL} is the absorption coefficient and d_{GL} the thickness of the

GL. The spectral variation of T_{GL} derived by Eq. (1) is reported in Fig. 4. For the sake of a better readability of the plot, the values of T_{GL} were binned over frequency ranges of ≈0.14 THz for TDS-1 and ≈0.4 THz for TDS-2, respectively, and the corresponding average values were evaluated. The standard deviation of the mean has been shown in Fig. 4 as vertical error bar, while the size of the bin is reported as horizontal error bar. For TDS-1, the horizontal error bar is smaller than the square symbol size.

We observe a clear difference for the different EM polarizations in the broad (0.25 ÷ 3.0 THz) spectral range strongly decreasing and almost overlapping at higher frequency values as a consequence of the commensurability of the effective impinging wavelength λ/n_{int} (where n_{int} is the refractive index of the metasurface) [33]. These results highlight a marked anisotropy in the transmission of THz radiation from the graphitic overlayer produced in fs laser irradiation of diamond and a direct correlation of the absorption coefficient with the orientation of the graphitic ripples generated on the diamond surface. By considering an average value of d_{GL}≈750 nm, the simple model of Eq. (1) allows deriving estimates of the absorption coefficients $\alpha_{GL,\perp} \approx 5 \times 10^5$ m^{-1} and $\alpha_{GL,\parallel} \approx 2 \times 10^6$ m^{-1} at frequency $\nu \approx 1$ THz. The values $\alpha_{GL,\parallel}$ is fairly consistent with the absorption coefficient of $\approx 1.7 \times 10^6$ m^{-1} at $\nu \approx 2.1$ THz reported by Komlenok et al. for uniform, conductive graphitized layers with submicron thickness produced by irradiating a CVD diamond plate with a KrF excimer laser [21].

In summary, we have realized both graphitized and black diamond samples treating thermal grade CVD polycrystalline diamond plates by fs laser surface texturing. The corresponding THz response has been investigated through the analysis of the transmittance in the spectral range (0.25 ÷ 6.0) THz. Our experimental findings demonstrate an interesting selective absorption of the graphitic overlayers produced on the diamond samples to polarized THz radiation in the range (0.25 ÷ 3) THz. The observed anisotropy in the response of the GD sample is associated to the presence of ripples over the graphitic overlayer. Such an anisotropy might be further improved by an appropriate selection of the graphitized-diamond layer features (e.g. thickness, ripples period, depth, etc.). Therefore, by exploiting fs laser irradiation one can selectively turn from dielectric to metallic-like specific micro-zones of the diamond plate and generate passive circuits and metasurfaces in THz band for the fabrication of robust, lightweight and broadband THz optical components. A better optical strength of diamond-based structures can be expected, which might render such an approach a viable route to the development of robust, compact, lightweight and broadband optical elements for ultra-intense THz fields applications.

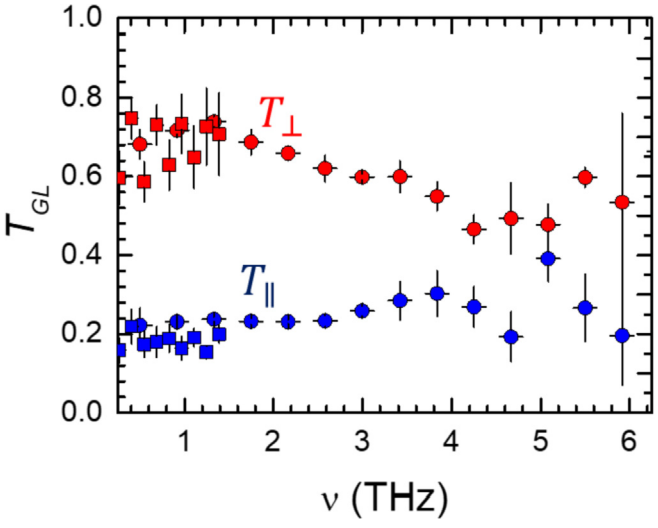

Fig. 4. Transmittance of the graphitized layer as recorded by using TDS-1 (squares) and TDS-2 (circles) setups for polarization parallel ($T_\parallel$, blue symbols) and orthogonal ($T_\perp$, red symbols) to the surface ripples. (A colour version of this figure can be viewed online.)

Declaration of competing interest

The authors declare that they have no known competing financial interests or personal relationships that could have appeared to influence the work reported in this paper.

References

[1] R.P. Mildren, J. Rabeau, Optical Engineering of Diamond, Wiley-VCH Verlag GmbH & Co. KGaA, 2013.
[2] V.I. Konov, Laser in micro and nanoprocessing of diamond materials, Laser Photon. Rev. 6 (2012) 739–766, https://doi.org/10.1002/lpor.201100030.
[3] B. Sotillo, V. Bharadwaj, J.P. Hadden, M. Sakakura, A. Chiappini, T.T. Fernandez, S. Longhi, O. Jedrkiewicz, Y. Shimotsuma, L. Criante, R. Osellame, G. Galzerano, M. Ferrari, K. Miura, R. Ramponi, P.E. Barclay, S.M. Eaton, Diamond photonics platform enabled by femtosecond laser writing, Sci. Rep. 6 (2016) 35566, https://doi.org/10.1038/srep35566.
[4] M.S. Komlenok, S.G. Tikhodeev, T. Weiss, S.P. Lebedev, G.A. Komandin, V.I. Konov, All-carbon diamond/graphite metasurface: experiment and modeling, Appl. Phys. Lett. 113 (2018), 041101, https://doi.org/10.1063/1.5037844.
[5] D. Trucchi, A. Bellucci, M. Girolami, M. Mastellone, S. Orlando, Surface texturing of CVD diamond assisted by ultrashort laser pulses, Coatings 7 (2017) 185, https://doi.org/10.3390/coatings7110185.
[6] M. Shimizu, Y. Shimotsuma, M. Sakakura, T. Yuasa, H. Homma, Y. Minowa, K. Tanaka, K. Miura, K. Hirao, Periodic metallo-dielectric structure in diamond, Optic Express 17 (2009) 46, https://doi.org/10.1364/OE.17.000046.
[7] T.V. Kononenko, P.N. Dyachenko, V.I. Konov, Diamond photonic crystals for the IR spectral range, Opt. Lett. 39 (2014) 6962, https://doi.org/10.1364/OL.39.006962.
[8] B. Sun, P.S. Salter, M.J. Booth, High conductivity micro-wires in diamond following arbitrary paths, Appl. Phys. Lett. 105 (2014) 231105, https://doi.org/10.1063/1.4902998.
[9] M. Girolami, L. Criante, F. Di Fonzo, S. Lo Turco, A. Mezzetti, A. Notargiacomo, M. Pea, A. Bellucci, P. Calvani, V. Valentini, D.M. Trucchi, Graphite distributed electrodes for diamond-based photon-enhanced thermionic emission solar cells, Carbon N. Y. 111 (2017) 48–53, https://doi.org/10.1016/J.CARBON.2016.09.061.
[10] R.S. Anwar, H. Ning, L. Mao, Recent advancements in surface plasmon polaritons-plasmonics in subwavelength structures in microwave and terahertz regimes, Digit. Commun. Netw. 4 (2018) 244–257, https://doi.org/10.1016/j.dcan.2017.08.004.
[11] S. Savo, E. Di Gennaro, A. Andreone, Superlensing properties of one-dimensional dielectric photonic crystals, Optic Express 17 (2009) 19848, https://doi.org/10.1364/oe.17.019848.
[12] J. Madéo, A. Margiolakis, Z.-Y. Zhao, P.J. Hale, M.K.L. Man, Q.-Z. Zhao, W. Peng, W.-Z. Shi, K.M. Dani, Ultrafast properties of femtosecond-laser-ablated GaAs and its application to terahertz optoelectronics, Opt. Lett. 40 (2015) 3388, https://doi.org/10.1364/ol.40.003388.
[13] Z. Zhao, Z. Song, F. Bai, W. Shi, Q.Z. Zhao, Terahertz refractive anisotropy on femtosecond laser pulse ablated semi-insulating gallium arsenide surface, Appl. Phys. Mater. Sci. Process 123 (2017) 1–6, https://doi.org/10.1007/s00339-017-0852-2.
[14] J. Bonse, S. Hohm, S.V. Kirner, A. Rosenfeld, J. Kruger, Laser-induced periodic surface structures-A scientific evergreen, IEEE J. Sel. Top. Quant. Electron. 23 (2017), https://doi.org/10.1109/JSTQE.2016.2614183.
[15] A.Y. Vorobyev, C. Guo, Direct femtosecond laser surface nano/microstructuring and its applications, Laser Photon. Rev. 7 (2013) 385–407, https://doi.org/10.1002/lpor.201200017.
[16] P. Calvani, A. Bellucci, M. Girolami, S. Orlando, V. Valentini, R. Polini, D.M. Trucchi, Black diamond for solar energy conversion, Carbon N. Y. 105 (2016) 401–407, https://doi.org/10.1016/J.CARBON.2016.04.017.
[17] Q. Wu, Y. Ma, R. Fang, Y. Liao, Q. Yu, X. Chen, K. Wang, Femtosecond laser-induced periodic surface structure on diamond film, Appl. Phys. Lett. 82 (2003) 1703–1705, https://doi.org/10.1063/1.1561581.
[18] A. Abdelmalek, B. Sotillo, Z. Bedrane, V. Bharadwaj, S. Pietralunga, R. Ramponi, E.H. Amara, S.M. Eaton, Origin of femtosecond laser induced periodic nanostructure on diamond, AIP Adv. 7 (2017), https://doi.org/10.1063/1.5001942.
[19] M. Forster, C. Huber, O. Armbruster, R. Kalish, W. Kautek, 50-nanometer femtosecond pulse laser induced periodic surface structures on nitrogen-doped diamond, Diam. Relat. Mater. 74 (2017) 114–118, https://doi.org/10.1016/j.diamond.2017.02.016.
[20] A.M. Zaitsev, Optical Properties of Diamond: a Data Handbook, Springer Berlin

Heidelberg, 2001.
[21] M.S. Komlenok, S.P. Lebedev, G.A. Komandin, A. Piqué, V.I. Konov, Fabrication and electrodynamic properties of all-carbon terahertz planar metamaterials by laser direct-write, Laser Phys. Lett. 15 (2018), 036201, https://doi.org/10.1088/1612-202X/AA8ED0.
[22] M. Martínez-Calderon, J.J. Azkona, N. Casquero, A. Rodríguez, M. Domke, M. Gómez-Aranzadi, S.M. Olaizola, E. Granados, Tailoring diamond's optical properties via direct femtosecond laser nanostructuring, Sci. Rep. 8 (2018) 14262, https://doi.org/10.1038/s41598-018-32520-0.
[23] A. Bellucci, P. Calvani, M. Girolami, S. Orlando, R. Polini, D.M. Trucchi, Optimization of black diamond films for solar energy conversion, Appl. Surf. Sci. 380 (2016) 8–11, https://doi.org/10.1016/J.APSUSC.2016.02.107.
[24] C. Casiraghi, A.C. Ferrari, J. Robertson, Raman spectroscopy of hydrogenated amorphous carbons, Phys. Rev. B 72 (2005), 085401, https://doi.org/10.1103/PhysRevB.72.085401.
[25] A.C. Ferrari, J. Robertson, Interpretation of Raman spectra of disordered and amorphous carbon, Phys. Rev. B 61 (2000) 14095–14107, https://doi.org/10.1103/PhysRevB.61.14095.
[26] J. Bonse, A. Hertwig, R. Koter, M. Weise, U. Beck, P. Reinstädt, M. Griepentrog, J. Krüger, M. Picquart, E. Haro-Poniatowski, Femtosecond laser pulse irradiation effects on thin hydrogenated amorphous carbon layers, Appl. Phys. Mater. Sci. Process 112 (2013) 9–14, https://doi.org/10.1007/s00339-012-7170-5.
[27] P.K. Bachmann, H.D. Bausen, H. Lade, D. Leers, D.U. Wiechert, N. Herres, R. Kohl, P. Koidl, Raman and X-ray studies of polycrystalline CVD diamond films, Diam. Relat. Mater. 3 (1994) 1308–1314, https://doi.org/10.1016/0925-9635(94)90143-0.
[28] L.J. van der Pauw, A method of measuring the resistivity and Hall coefficient on lamellae of arbitrary shape, Philips Res. Rep. 20 (1958) 220–224.
[29] A. Orsini, A. Bellucci, M. Girolami, M. Mastellone, S. Orlando, G. Prestopino, V. Valentini, S. Salvatori, D.M. Trucchi, Electrical conductivity of double textured black diamond films from RT to 800 K, Diam. Relat. Mater. 93 (2019) 1–7, https://doi.org/10.1016/J.DIAMOND.2019.01.011.
[30] A. Rubano, S. Mou, L. Marrucci, D. Paparo, Terahertz hyper-Raman time-domain spectroscopy, ACS Photonics 6 (2019) 1515–1523, https://doi.org/10.1021/acsphotonics.9b00265.
[31] J. Zhang, L. Zhang, W. Xu, Surface plasmon polaritons: physics and applications, J. Phys. D Appl. Phys. 45 (2012) 113001, https://doi.org/10.1088/0022-3727/45/11/113001.
[32] R.W. Wood, Anomalous diffraction gratings, Phys. Rev. 48 (1935) 928–936, https://doi.org/10.1103/PhysRev.48.928.
[33] G.P. Papari, C. Koral, A. Andreone, Geometrical dependence on the onset of surface plasmon polaritons in THz grid metasurfaces, Sci. Rep. 9 (2019) 924, https://doi.org/10.1038/s41598-018-36648-x.

S. Amoruso*, A. Andreone
Dipartimento di Fisica, Università di Napoli Federico II, Complesso Universitario di Monte S. Angelo, Via Cintia, I-80126, Napoli, Italy

CNR-SPIN, SuPerconducting and other INnovative materials and devices Institute, UOS Napoli, Complesso Universitario di Monte S. Angelo, Via Cintia, I-80126, Napoli, Italy

A. Bellucci
CNR-ISM, Institute for Structure of Matter ISM-CNR, DiaTHEMA Lab, Via Salaria km 29.300, Monterotondo Scalo, (RM), Italy

C. Koral
Istituto Nazionale di Fisica Nucleare, Sezione di Napoli, via Cintia, I-80126, Napoli, Italy

M. Girolami
CNR-ISM, Institute for Structure of Matter ISM-CNR, DiaTHEMA Lab, Via Salaria km 29.300, Monterotondo Scalo, (RM), Italy

M. Mastellone
CNR-ISM, Institute for Structure of Matter ISM-CNR, DiaTHEMA Lab, Via Salaria km 29.300, Monterotondo Scalo, (RM), Italy

S. Mou
Dipartimento di Fisica, Università di Napoli Federico II, Complesso Universitario di Monte S. Angelo, Via Cintia, I-80126, Napoli, Italy

S. Orlando
CNR-ISM, Institute for Structure of Matter ISM-CNR, DiaTHEMA Lab, Via Salaria km 29.300, Monterotondo Scalo, (RM), Italy

G.P. Papari
Dipartimento di Fisica, Università di Napoli Federico II, Complesso Universitario di Monte S. Angelo, Via Cintia, I-80126, Napoli, Italy

D. Paparo
CNR-ISASI, Institute of Applied Science & Intelligent Systems (ISASI) 'E. Caianiello', Via Campi Flegrei 34, 80078, Pozzuoli, (NA), Italy

R. Polini
Università di Roma "Tor Vergata", Dipartimento di Scienze e Tecnologie Chimiche, Via della Ricerca Scientifica 1, 00133, Roma, Italy

A. Rubano
Dipartimento di Fisica, Università di Napoli Federico II, Complesso Universitario di Monte S. Angelo, Via Cintia, I-80126, Napoli, Italy

CNR-ISASI, Institute of Applied Science & Intelligent Systems (ISASI) 'E. Caianiello', Via Campi Flegrei 34, 80078, Pozzuoli, (NA), Italy

A. Santagata, V. Serpente, V. Valentini, D.M. Trucchi
CNR-ISM, Institute for Structure of Matter ISM-CNR, DiaTHEMA Lab, Via Salaria km 29.300, Monterotondo Scalo, (RM), Italy

* Corresponding author. Dipartimento di Fisica, Università di Napoli Federico II, Complesso Universitario di Monte S. Angelo, Via Cintia, I-80126, Napoli, Italy.
E-mail address: salvatore.amoruso@unina.it (S. Amoruso).

9 January 2020
Available online 10 March 2020